Ionics (2020) 26:3919–3927
https://doi.org/10.1007/s11581-020-03538-0

ORIGINAL PAPER

Dual carbon decorated $Na_3TiMn(PO_4)_3$ as an advanced cathode for sodium-ion batteries

Xuewen Sun[1] · Taosheng Wang[1] · Wei Zhang[1] · Huangxu Li[1,2] · Yanqing Lai[1] · Zhian Zhang[1]

Received: 12 February 2020 / Revised: 7 March 2020 / Accepted: 13 March 2020 / Published online: 8 April 2020

Abstract

Na super ionic conductor (NASICON)-type $Na_3V_2(PO_4)_3$ (NVP) is a high-energy sodium-ion battery material for sodium-ion batteries (NIBs), which has a high theoretical specific capacity, structural stability, and high safety performance. However, in order to promote its practical applications, it is imperative to replace vanadium with other low-cost and rich elements on earth. Therefore, NASICON-$Na_3TiMn(PO_4)_3$ (NTMP) is more attractive due to its higher voltage platform and lower toxicity. However, its low electrical conductivity, unsatisfactory rate performance, and cycle life limit its practical application. Herein, the feasibility to realize advanced rate capability and long durability through dual carbon decoration strategy that in situ embedding single-walled carbon nanotubes (SWCNT) into the bulk of $Na_3TiMn(PO_4)_3$@C is reported. The elaborately designed $Na_3TiMn(PO_4)_3$@C@SWCNT can deliver an initial charge capacity of 112 mA h g^{-1} at a current rate of 0.1 C with a long durability over 1000 cycles at 2 C. This progress can be benefited from the improvement of the electrical conductivity of the materials brought by the cross-linked conductive network and the robust structure.

Keywords Sodium-ion batteries · Single-walled carbon nanotubes · $Na_3TiMn(PO_4)_3$ · Carbon coating

Introduction

With the attention paid to the consumption of nonrenewable fossil fuels increasing, the storage of clean energy has become a great concern for governments and scientists [1–3]. Since the sodium is rich in resources and low in cost, sodium-ion batteries (NIBs) are one of the most promising options in large energy storage systems [4–7]. However, the insertion/extraction of Na^+ ions from the active material is often accompanied by a large volume change caused by the large radius of sodium ions, making the development of stable electrode materials a challenge. Besides, low energy/power density, slow sodium mobility, and short life span on the electrode (especially cathode) materials still need to be addressed [8–12]. To solve these problems, researchers strive to find suitable cathode materials, including Prussian blue analogs (Pba), layered transition metal oxide, and polyanionic compounds, which have been widely studied. Layered transition metal oxide materials have high theoretical specific capacity, but the structure is not stable and their cycle life is not ideal [9–11]. Due to poor thermal stability and low volume density of Prussian blue and cyanide toxicity, it limits its application [12–14]. In this context, polyanionic materials are widely investigated because of their robust crystal framework, high thermal stability, moderate capacity, adjustable high redox potential, and high energy density [15–21].

The $Na_xM_y(PO_4)_3$ (M = transition metal) series of NASICON structure has been widely used as an electrode material for rechargeable batteries due to its good ion diffusion channels and strong frame structure [20, 21]. In particular, NASICON-structured $Na_3V_2(PO_4)_3$ has been considered as a hot research spot [22–27]. However, its large-scale application is limited by the expensive and toxic vanadium. In this aspect, researchers have focused on partially replacing V with other low-cost and environment-friendly elements [28]. Due to the low cost and environmentally friendly manganese, manganese-based materials have potential for large-scale applications, and the addition of manganese also brings higher operating voltage [29]. Due to the Jahn-Teller effect of manganese, we need to add other elements to stabilize the lattice,

✉ Zhian Zhang
zhangzhian@csu.edu.cn

[1] School of Metallurgy and Environment, Central South University, Changsha 410083, People's Republic of China

[2] Department of Chemistry, City University of Hong Kong, Kowloon, Hong Kong, China

in order to make better use of the high voltage platform of manganese. $Na_3TiMn(PO_4)_3$ as cathode shows good application prospects because it is greener, is more lower in cost, and has higher voltage platform [18, 30, 31]. However, the poor electronic conductivity limits the electrochemical performance of $Na_3TiMn(PO_4)_3$, which makes the theoretical performance difficult to realize. We know that the introduction of conductive carbon is a common method to increase the conductivity of electrode materials. However, a simple carbon coating is not so satisfactory. SWCNT is a very good conductivity material that can lead to a significant increase in the performance of the material used in battery [32–38].

In this work, we successfully embedded single-walled carbon nanotubes (SWCNT) into the bulk of carbon-coated $Na_3TiMn(PO_4)_3$ (NTMP@C) through sol-gel method. We elaborately designed $Na_3TiMn(PO_4)_3$@C@SWCNT (NTMP@C@SWCNT) that can deliver an initial charge capacity of 112 mA h g^{-1} at 0.1 C with a long cycle life of 1000 cycles at 2 C. This progress has benefited from the increased electrical conductivity of the materials brought about by the cross-linked conductive network and the sturdy structure.

Experimental section

Synthesis of $Na_3TiMn(PO_4)_3$@C@SWCNT composite

$Na_3TiMn(PO_4)_3$@C@SWCNT composite was prepared by simple sol-gel method. First, stoichiometric citric acid, sodium acetate, manganese acetate, and $NH_4H_2PO_4$ were dissolved in 20 ml deionized water in molar ratios. After stirring the solution at 80 °C for 30 min. Isopropyl titanate and a little bit SWCNT were then dissolved in 20 ml anhydrous ethanol and ultrasound for 1 h. The anhydrous ethanol solution was then slowly dripped into the deionized water solution. The mixed solution was continuously stirred for 6 h to dry the solvent under the condition of 80 °C oil bath to obtain the gel. The resulting gel was then transferred to the vacuum oven and heated to 120 °C for 3 h. Then, the dry gel was ground and calcinated under an argon atmosphere at 650 °C for 10 h to obtain the $Na_3TiMn(PO_4)_3$@C@SWCNT composite. The specific steps are presented in Fig. 1. Its crystal structure is also shown in Fig. 1. $Na_3TiMn(PO_4)_3$@C is prepared in the same way as described above except adding any SWCNT.

Materials characterization

The purity of $Na_3TiMn(PO_4)_3$@C@SWCNT composite was researched by X-ray diffraction with a Cu-Kα radiation at room temperature, and the scan rate is 1° min^{-1}, and range is 10 to 80° (Bruker D8 Advance). The refinement is performed by GSAS software, and the crystal structure is visualized by VESTA. Field emission scanning electron microscope was used to characterize its particle size and morphology (SEM, Zeiss Sigma HD). Transmission electron microscopy was used to observe the microstructure of particle materials (TEM, JEM-2100, Japan). Carbon content of the $Na_3TiMn(PO_4)_3$@C@SWCNT material was researched by thermogravimetric (TG) analysis. X-ray photoelectron spectroscopy (XPS, ESCALAB 250Xi) was analyzed to determine the valence state of the elements. The nitrogen isothermal adsorption-desorption analysis was performed to reveal the Brunauer-Emmett-Teller (BET) specific surface area of the samples (Micromeritics ASAP 2020 instrument, Norcross, GA, USA). Raman spectroscopy was used to analyze the degree of graphitization of carbon (LabRAM HR Evolution).

The electrochemical performance of the materials was investigated using CR2032 assembled batteries. The cathode electrode is composed of 70% by weight of active material, 10% by weight of polyvinylidene fluoride, and 20% by weight of carbon black. The sodium metal was employed as negative electrode, 1.0 M $NaClO_4$ was dissolved in a PC with fluoroethylene carbonate (5 vol%) which was added to form an electrolyte. Constant current charge and discharge, long cycle, and rate performance were measured on a battery test system (CT2001A), and the potential range is 2.5–4.2 V. Cyclic voltammetry (CV) tests were performed on the PARSTAT 2273 electrochemical workstation from 2.5 to 4.2 V.

Results and discussion

Synthesis of NTMP@C@SWCNT and control of its particle size by a feasible sol-gel method, as schematically illustrated in Fig. 1. Isopropyl titanate and SWCNT which are conducive to the formation of SWCNT conductive network, are evenly dispersed in ethanol. Citric acid acts as carbon source and chelating agent. The B solution was dropped into the A solution and stirred uniformly, then the solvent was evaporated, and the material was sintered at 650 °C for 10 h. The crystal structure of the material is drawn from the refined results shown in Fig. 1. The specific synthesis steps of NTMP@C@SWCNT and its crystal structure are shown in Fig. 1. From this figure, NASICON-type $Na_3TiMn(PO_4)_3$ is formed on a three-dimensional framework MnO_6 or TiO_6 octahedron that share all the PO_4 tetrahedron angle. The polyanionic phosphate skeleton gives $Na_3TiMn(PO_4)_3$ excellent structural stability and inherent safety.

The Rietveld refinement of the particle material was primarily employed (Fig. 2a). X-ray diffraction peaks marked with a triclinic structure with R3c as a space group. The fitting result is satisfactory, and the reliability coefficient is Rp = 11.0%. The lattice parameters are a = 8.821812 Å, b = 8.821812 Å, c = 21.738842 Å, α = 90.0°, β = 90.0°, and γ = 120.0°. NASICON-type $Na_3TiMn(PO_4)_3$ is a skeleton

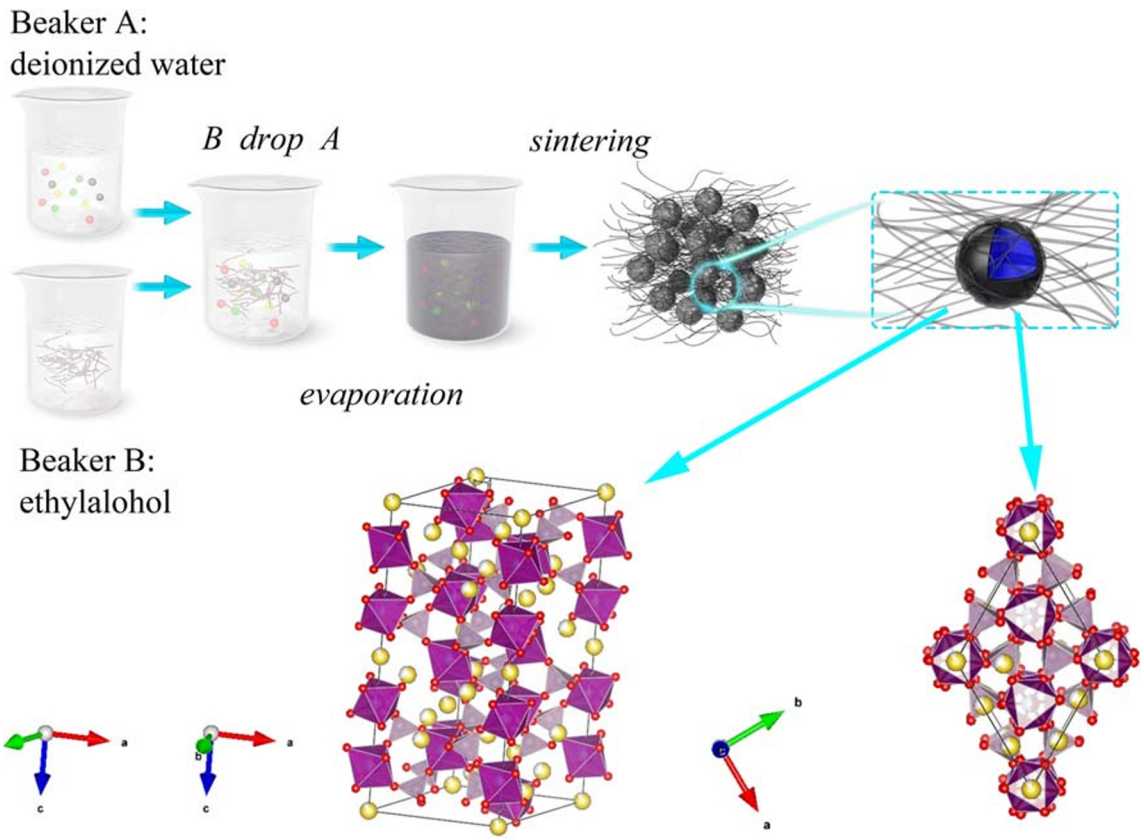

Fig. 1 Preparation process of the cathode material and the crystal structure of the cathode material

structure composed of MnO_6 or TiO_6 octahedron with common angle and PO_4 tetrahedral elements, and there are wide open channels between them. Since the stability of PO_4, backbone phosphate polyanion has a satisfactory structural stability and inherent safety, which makes the redox of the transition metal become stronger. And sodium ions occupy two different sites: the sixfold coordination N1 site and the eightfold coordination N2 site in the skeleton structure. During charging and discharging, sodium ions located at N1 site are fixed, and sodium ions located at N2 site can be extracted and inserted into electrochemical activity. Due to the robust binding of the sodium ion located at the N1 site to the coordinating oxygen atom, only the sodium ion located at the N2 site can be extracted and inserted for electrochemical activity. Using Mn^{2+}/Mn^{3+} and Mn^{3+}/Mn^{4+} redox coupling agents to reversibly pull or insert two sodium ions at the N2 site, a theoretical capacity of 117 mA h g^{-1} can be obtained, and it also has two voltage platforms of 3.6 V and 4.1 V. The fitting result and XRD indicate that NTMP material had been successfully synthesized [30, 31]. XPS was used to discern the NTMP@C@SWCNT material. The existence of Na, Mn, Ti, P, O, and C were revealed by the wide-range spectrum of XPS (Fig. 2b). The reduction and oxidation of manganese are accompanied by the insertion and extraction of sodium ions. The two sodium ions can be extracted and inserted from NTMP by using Mn^{3+}/Mn^{2+} and Mn^{4+}/Mn^{3+} redox coupling. Moreover, from Fig. 2c and d, manganese has two oxidation states of Mn and two oxidation states of Ti that exist simultaneously in NTMP@C@SWCNT. And Mn^{2+} accounts for about 1/4 of the total Mn, and Ti^{3+} accounts for about 1/3 of the total Ti.

The images of SEM and TEM reveal the morphology of the samples. From Fig. 3a, b, and c, the prepared material (NTMP@C@SWCNT) structure is not very regular, SEM (Fig. 3c) indicates that the microspheres are made of NTMP nanoparticles and SWCNT, and the SWCNTs constitute a 3-D conductive network visible on their surfaces. In addition, there is a clear carbon layer structure on the surface of the material. TEM imaging (Fig. 3d, e) demonstrates the relationships between the prepared materials, amorphous carbon layers, and 3-D nanotube networks. HRTEM images (Fig. 3f) reveal the lattice structure of the material and the lattice fringes of SWCNTs that are also clearly visible. In order to make sure the existence and distribution of every element, EDS mapping was performed (Fig. 3g–i). That clearly demonstrates that all elements (C, Ti, Na, Mn, P) are very homogeneous. In this composite structure, the surface of the material synthesized by the one-step method is coated with a uniform carbon layer, and the carbon-coated material is also attached to a three-dimensional conductive network constituting SWCNT. The cross-linking between SWCNT and carbon coating speed up electron transfer between multiple particles. In contrast, Fig. 4 reveals the morphology of the NTMP@C. From Fig. 4a and c,

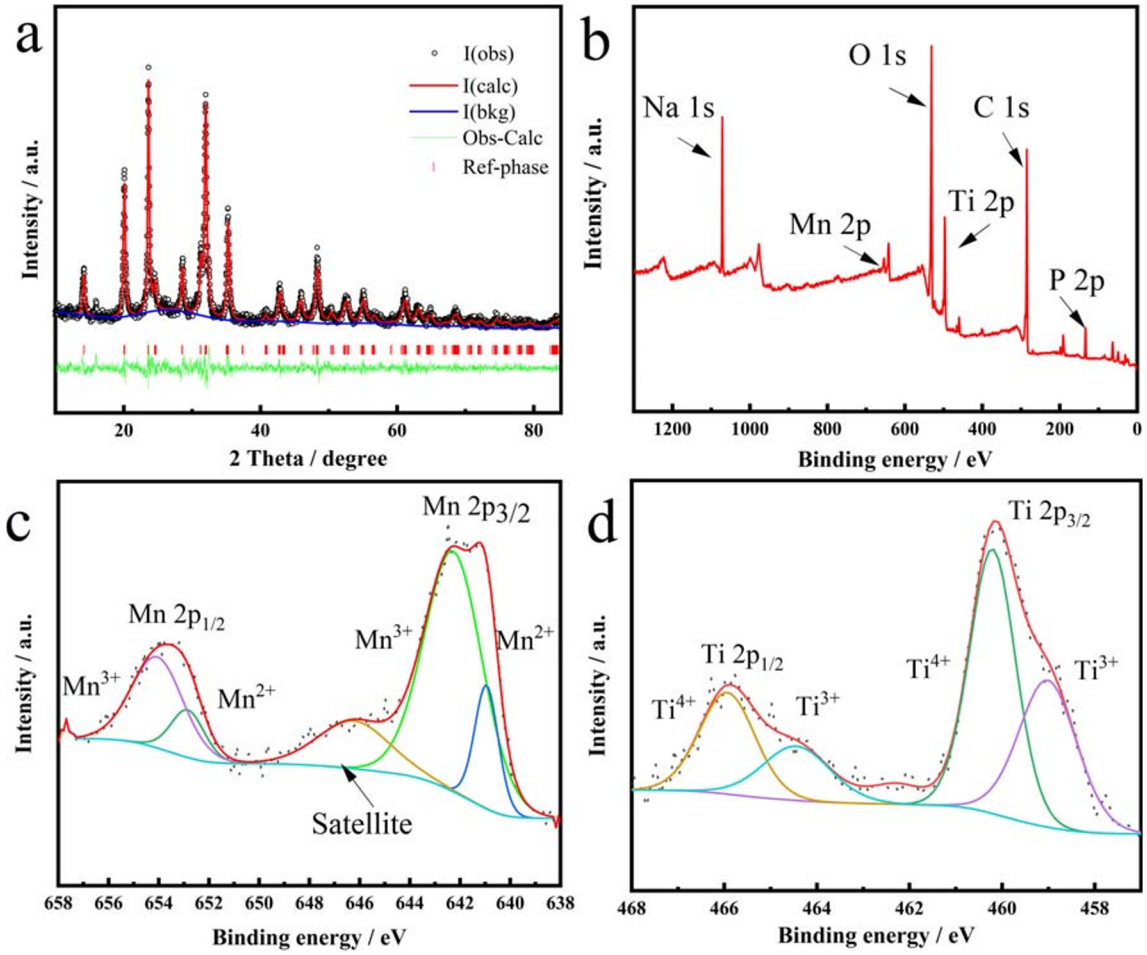

Fig. 2 **a** Rietveld refinement of the XRD pattern of the NTMP@C@SWCNT material. **b** XPS spectra in a wide-range scanning core-level spectra of **c** Mn 2p and **d** Ti 2p

the prepared material (NTMP@C) structure is also not very regular, SEM (Fig. 4c) indicates that the microspheres are made of NTMP nanoparticles, and there is no SWCNT. From Fig. 4b and d, the lattice structure of the NTMP@C and the carbon-coated morphology of the material are exhibited. Therefore, due to the joint contribution of the carbon-coating layer and the three-dimensional conductive network of SWCNT, the conductivity of the composite material is significantly improved. The surface of the material is uniformly covered by carbon layer, and the cross-linking between SWCNT accelerates electron transfer between multiple material particles. Due to the combined effect of the carbon coating and the SWCNT three-dimensional conductive network, the electrical conductivity and the electrochemical performance of the prepared material are significantly improved.

Figure 5a demonstrates thermogravimetric test of the NTMP@C@SWCNT and the NTMP@C, the carbon content of 19.7 wt.% and 17.5 wt.% in the NTMP@C@SWCNT, and the NTMP@C, respectively. Figure 5b demonstrates the result test of Raman spectroscopy. Raman spectroscopy reveals the presence of highly graphitized carbon to distinguish between disordered and graphitized carbon. The graphitization of carbon materials is evaluated by the intensity ratio of the D-band and G-band. The ID/IG values of NTMP@C and NTMP@C@ SWCNT are 0.90 and 0.93, respectively, which are close to each other. It indicates that the two have similar graphitization degrees. Figure 5c shows the pore distribution and specific surface area of the NTMP@C@SWCNT. The specific surface area of the material is 12.95 $m^2\ g^{-1}$. The average pore volume of the material is 2.51 nm. The results show that the sample has an internal mesoporous structure, so rich electrolyte can promote penetration of the pore structure, thus affecting the rate performance of the electrode.

The electrochemical properties of all NTMP samples were discussed in detail, as shown in Fig. 6. The charge and discharge curves of the NTMP@C@SWCNT and NTMP/C (Fig.6a) were tested at a C-rate of 0.1 C (1 C = 80 mA g^{-1}), and the electrode voltage window is from 2.5 to 4.2 V (vs Na^+/Na). Two distinct voltage platforms (vs Na/Na^+) have been observed around 3.6 and 4.1 V corresponding to the redox of

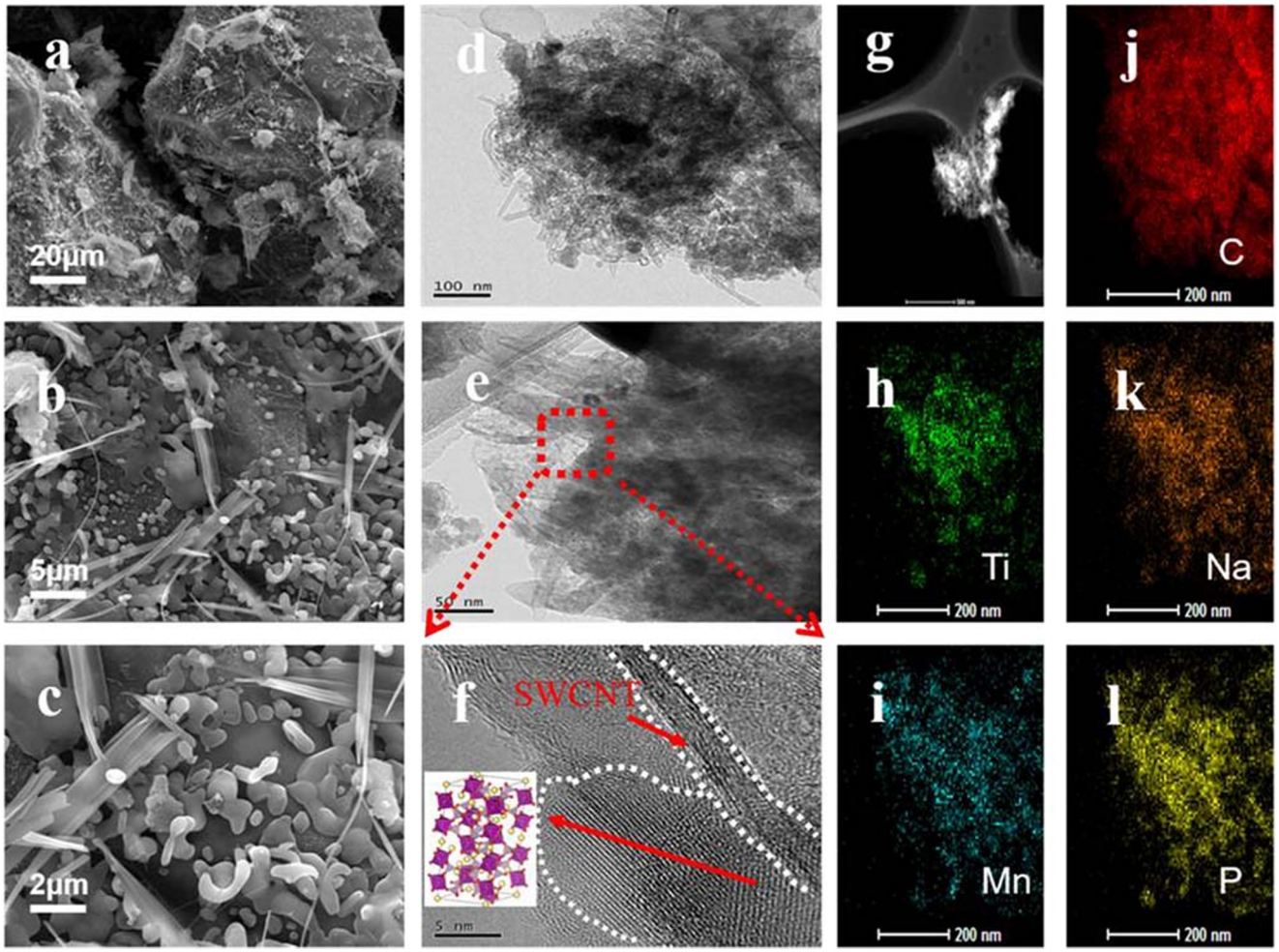

Fig. 3 Physical and chemical characterization of the samples. **a**, **b**, **c** SEM. **d**, **e** TEM images. **f** HRTEM image. **g**–**i** The corresponding elemental of mappings

Mn^{3+}/Mn^{2+} and Mn^{4+}/Mn^{3+} pairs, respectively. NTMP@C@SWCNT can deliver a capacity of 79 mA h g^{-1} higher than 70 mA h g^{-1} (NTMP@C). Due to the 3-D conductive network formed by SWCNT to boost the electronic conductivity of the material, it can get a higher discharge capacity observed in the NTMP@C@SWCNT. The CV curve of the NTMP@C@SWCNT electrodes was tested (Fig. 6b). Its test condition is that the scanning rate is 0.1 mV s^{-1} and the voltage range is 2.5–4.2 V. In NTMP, the redox peak centered on 3.6 V approaches to the equilibrium potential of Mn^{2+}/Mn^{3+} redox dipole. The center of the peak is approximately the redox couple of Mn^{3+}/Mn^{4+} corresponding to 4.1 V. The CV curves were almost overlapped from the second cycle, revealing that the extraction/insertion of sodium ions from NTMP has acceptable reversibility.

From Fig. 6c, the NTMP@C can deliver a capacity of 54, 50, 41, 31, and 21 mA h g^{-1} at 0.1, 0.2, 0.5, 1, and 2 C, respectively. In contrast, NTMP@C@SWCNT can deliver a capacity of 64, 59, 52, 47, and 43 mA h g^{-1} at 0.1, 0.2, 0.5, 1, and 2 C, respectively. It can be understood that NTMP@C@SWCNT exhibits better rate performance. When the rate capability was restored from 2 to 0.1 C, its reversible capacity was restored to 61 mA h g^{-1}, which explained that this material has good reversibility. At the discharge rate of 2 C, the NTMP@C@SWCNT can deliver a capacity of 41 mA h g^{-1}; in contrast the NTMP@C has 21 mA h g^{-1}. In addition, the capacity maintenance of the NTMP@C@SWCNT and the NTMP@C after 500 cycles at 2 C are more than 95% and 90%, respectively. This shows that the material shows good cycle stability during the charge and discharge process. Moreover, the 3-D structure formed by SWCNT cross-linking enhances the performance of cathode materials. However, due to the influence of temperature, it can be seen that the material will fluctuate a little during the cycle.

Figure 7 demonstrates long cycle stability of the NTMP@C@SWCNT. Impressively, Fig. 7 reveals that the initial capacity of this NTMP@C@SWCNT electrode is 43 mA h g^{-1} at the discharge rate of 2 C and maintains a significant capacity of 41 mA h g^{-1} after 1000 cycles. The coulomb efficiency of the material shows good stability at

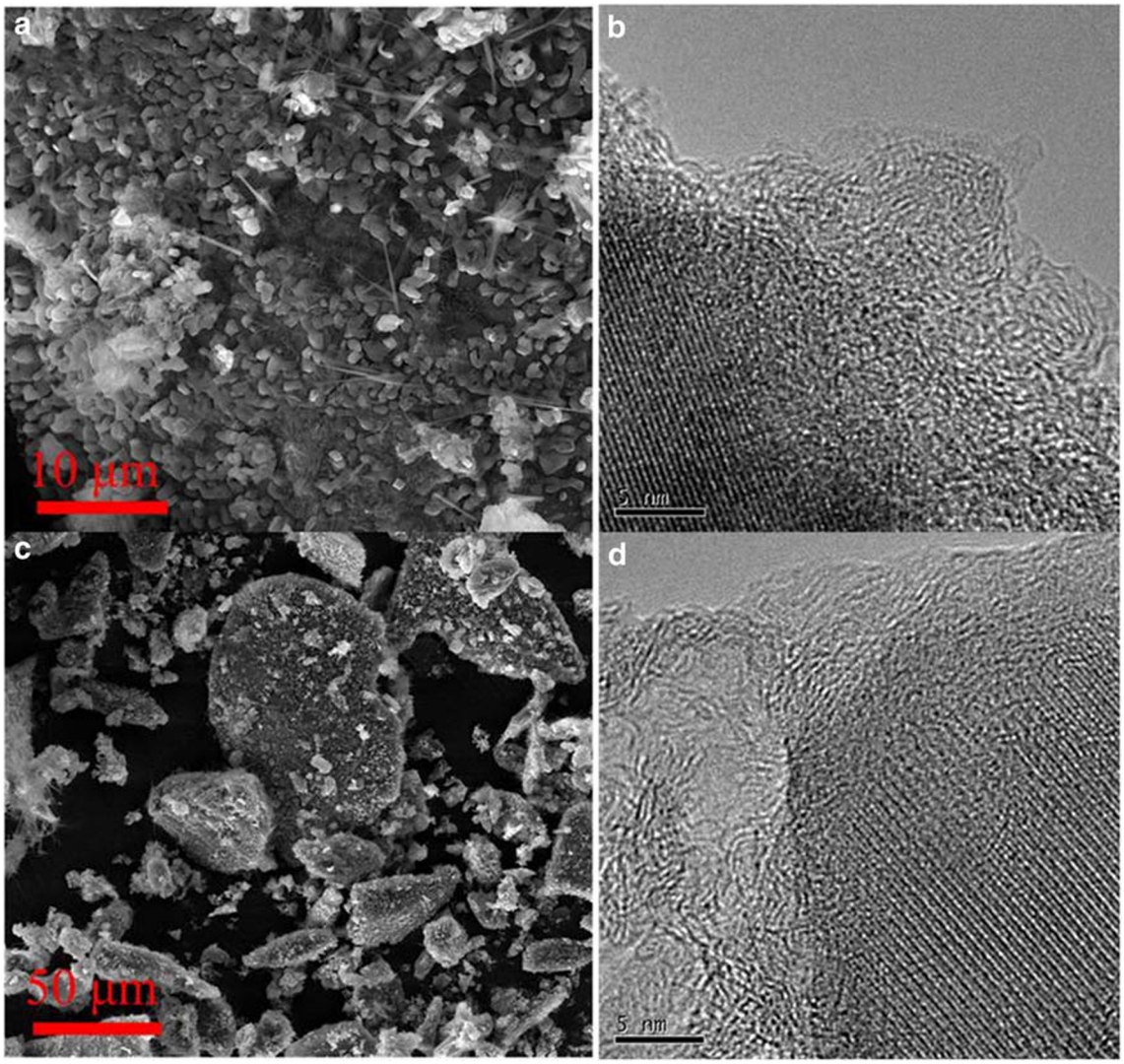

Fig. 4 Physical and chemical characterization of the NTMP@C. **a**, **c** SEM. **b**, **d** HRTEM images

the beginning, and the coulomb efficiency remains at about 100%, showing remarkable cyclability. It is expected to become a high-voltage environmentally friendly cathode material having a long life cycle. It is possible to achieve the goal of large-scale energy storage applications.

To further unearth the Na migration kinetics in the NTMP@C@SWCNT electrode, the galvanostatic intermittent titration technique (GITT) has been used. The transformation of the effective diffusion coefficient of Na^+ ions (D_{Na^+}) for NTMP@C@SWCNT electrodes is

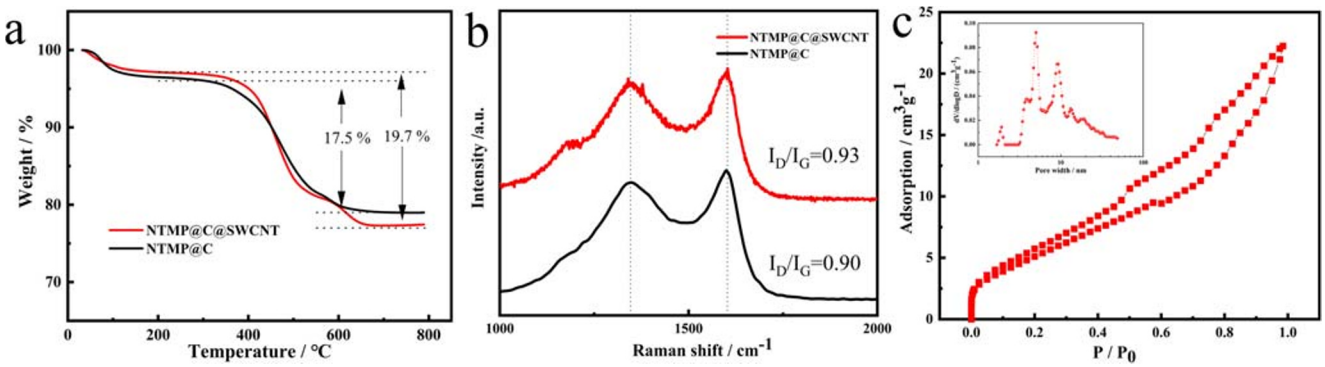

Fig. 5 **a** TG of the NTMP@C and the NTMP@C@SWCNT materials. **b** Raman spectra of the NTMP@C and the NTMP@C@SWCNT. **c** The nitrogen adsorption-desorption curve and pore-size distribution of the NTMP@C@SWCNT

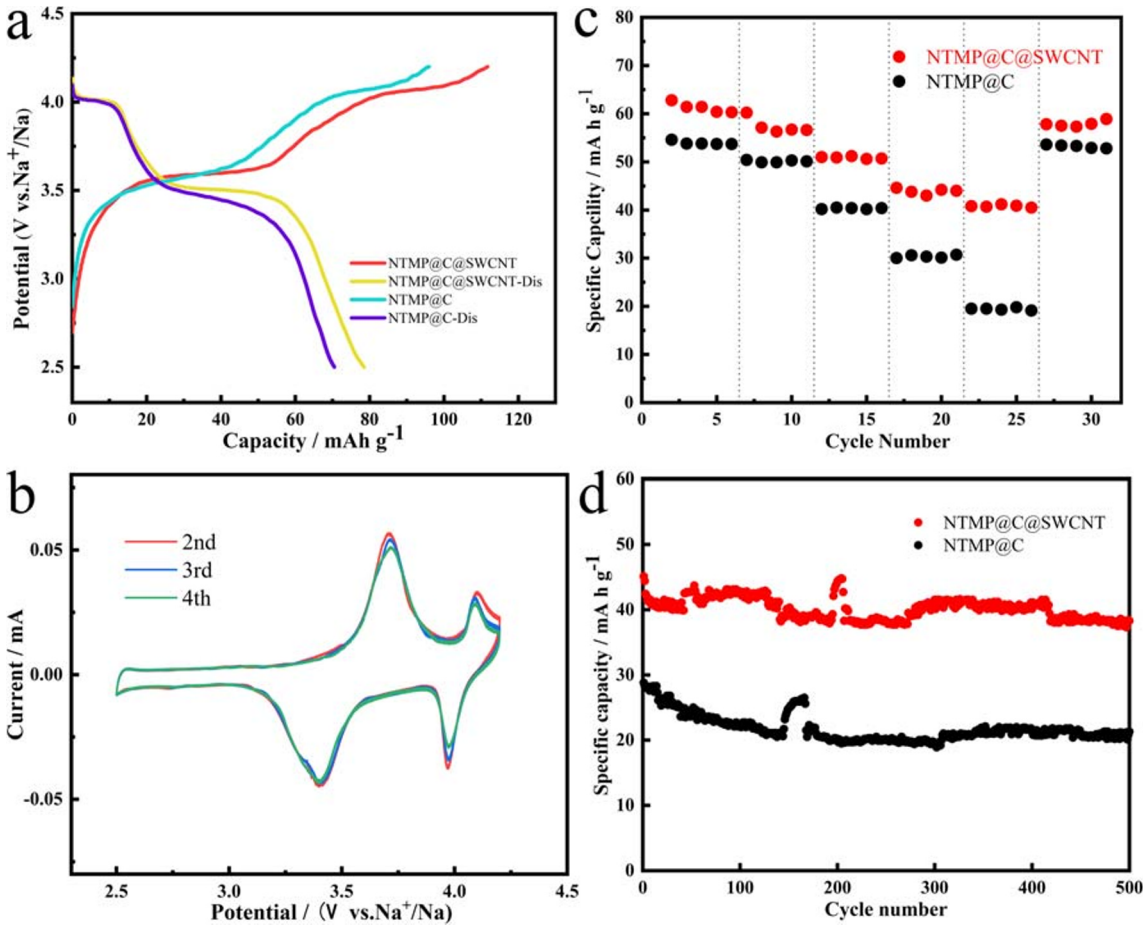

Fig. 6 Electrochemical performances of the as-prepared cathodes. **a** Galvanostatic charge/discharge profiles in the first cycle. **b** The CV of the NTMP@C@SWCNT. **c** Charge/discharge at different rates. **d** Cycle performance at 2 C

displayed in Fig. 8a. The value of the ion diffusion coefficient is about 10^{-8}–10^{-12} cm^2 s^{-1} indicating that this NASICON-type material has the characteristics of easy migration. Otherwise, TEM image after material cycling is shown in Fig. 8b. It is known that the 3-D structure of SWCNT cross-linked has not changed after cycling. The material is evenly attached to the three-dimensional structure. The prominent electrochemical performance of this NTMP@C@SWCNT cathode composite can come down to the following elements: First of all, the carbon-coating layer can enhance the electronic conductivity of individual NTMP particle.

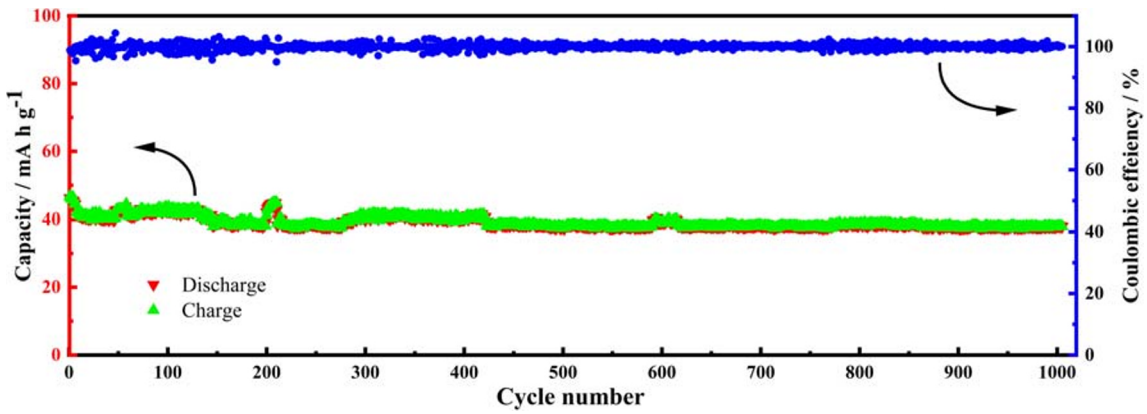

Fig. 7 Cycling capability of the NTMP@C@SWCNT under a high rate of 2 C

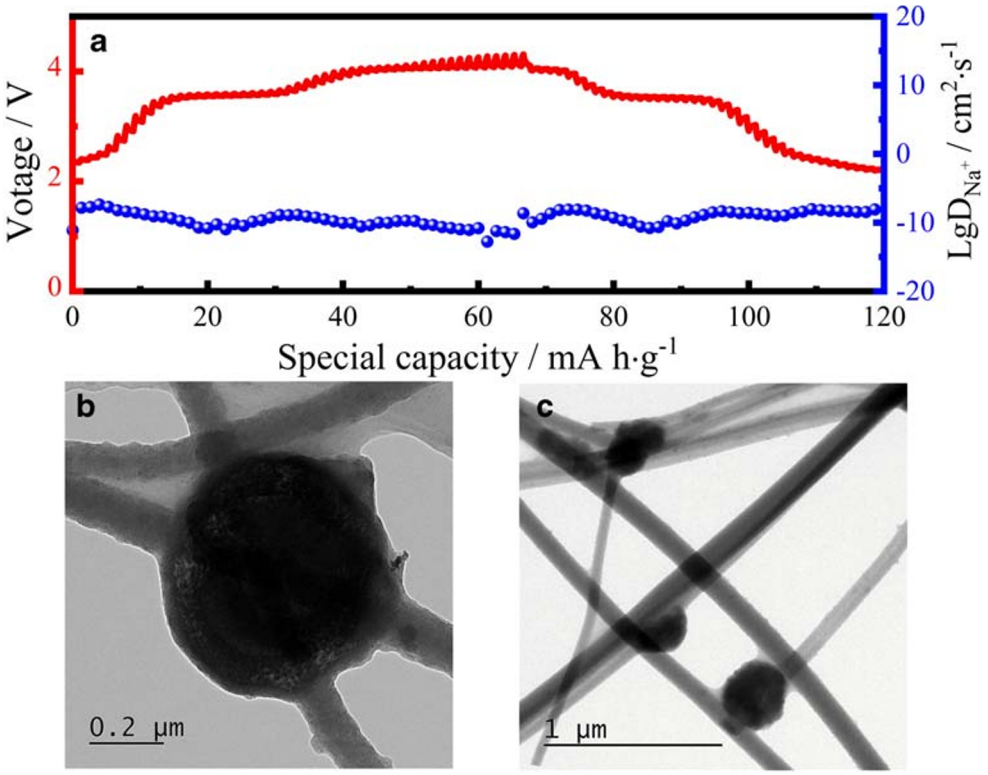

Fig. 8 **a** GITT profiles, Na^+ diffusion coefficient and overpotentials of the NTMP@C@SWCNT. **b**, **c** TEM after the cycle

Secondly, the structure of the amorphous carbon layer reinforces the contact between the NTMP particle and the electrolyte, which are advantageous to quicken Na^+ transportation rate through the carbon-coated layer. Lastly, the most important thing is due to the close contacts between the active materials, and the SWCNT 3-D conductive network can enhance electron migration between multiple NTMP particles. Consequently, the electrochemical characteristics of NTMP@C@SWCNT are more excellent than NTMP@C.

Conclusion

In summary, NTMP@C and NTMP@C@SWCNT with NASICON-structured structure were synthesized by a feasible sol-gel method. Both materials exhibit stable cycling performance, with voltage platforms of 3.6 V and 4.1 V, respectively. Among them, NTMP@C@SWCNT has better performance. When the discharge rate is 2 C, the reversible capacity is about 41 mA h g^{-1}, and the cycling performance of the material is stable. This excellent electrochemical performance is attributed to the conductive network formed by SWCNT cross-linking. Due to its green system, stable material structure, high voltage, and long cycle characteristics, $Na_3TiMn(PO_4)_3$ has a good application prospect in the future large-scale energy storage field.

Funding information The authors thank the financial support of the Fundamental Research Funds for the Central Universities of Central South University (2018zzts426).

References

1. Chu S, Majumdar A (2012) Opportunities and challenges for a sustainable energy future. Nature 488:294–303
2. Armand M, Tarascon J-M (2008) Building better batteries. Nature 45:1652–1657
3. Goodenough J-B (2014) Electrochemical energy storage in a sustainable modern society. Energy Environ Sci 7:14–18
4. Zhi, Xu, et al Ceramics International. 10.1016/j.ceramint.2019.10181
5. Li H, Xu M, Gao C, Zhang W, Zhang Z, Lai Y, Jiao L (2019) Highly efficient, fast and reversible multi-electron reaction of $Na_3MnTi(PO_4)_3$ cathode for sodium-ion batteries. Energy Storage Mater 16:383–390
6. Xiang X, Zhang K, Chen J (2015) Recent advances and prospects of cathode materials for sodium-ion batteries. Adv Mater 27:5343
7. Li Y, Lu Y, Zhao C, Hu Y-S, Titirici MM, Li H, Huang X, Chen L (2017) Recent advances of electrode materials for low-cost sodium-ion batteries towards practical application for grid energy storage. Energy Storage Mater 7:130–151
8. Xu GL et al (2018) Challenges in developing electrodes, electrolytes, and diagnostics tools to understand and advance sodium-ion batteries. Adv Energy Mater 8:1702403
9. Yabuuchi N, Kajiyama M, Iwatate J et al (2012) P2-type $Na_x[Fe_{1/2}Mn_{1/2}]O_2$ made from earth-abundant elements for rechargeable Na batteries. Nature Mater 11:512–517
10. Wang PF et al (2017) Honeycomb-ordered $Na_3Ni_{1.5}M_{0.5}BiO_6$ (M = Ni, Cu, Mg, Zn) as high voltage layered cathodes for sodium-ion batteries. ACS Energy Lett:2715–2722

11. Slater MD, Kim D, Lee E, Johnson CS (2013) Sodium-ion batteries. Adv Funct Mater 23:947–958
12. Jiang Y, Yu S, Wang B, Li Y, Sun W, Lu Y et al (2016) Prussian blue @C composite as an ultrahigh-rate and long-life sodium-ion battery cathode. Adv Funct Mater 26:5315–5321
13. Wu X, Sun M, Guo S, Qian J, Liu Y, Cao Y et al (2015) Vacancy-free Prussian blue nanocrystals with high capacity and superior cyclability for aqueous sodium-ion batteries. Chem Nano Mat 1(3):188–193
14. Peng J, Wang J, Yi H, Hu WJ, Huang Y (2018) A dual-insertion type sodium-ion full cell based on high-quality ternary-metal Prussian blue analogs. Adv Energy Mater 8:1702856
15. Lei P, Liu K, Wan X, Luo D, Xiang X (2019) Ultrafast Na intercalation chemistry of $Na_2Ti_{3/2}Mn_{1/2}(PO_4)_3$ nanodots planted in a carbon matrix as a low cost anode for aqueous sodium-ion batteries. Chem Commun 55:509–512
16. Kim J, Park I, Kim H, Park KY, Park YU, Kang K (2016) Tailoring a new 4v-class cathode material for Na-ion batteries. Adv Energy Mater 6:1502147
17. Jian Z, Hu YS, Ji X, Chen W (2017) NASICON-structured materials for energy storage. Adv Mater 29:1601925
18. Gao H, Goodenough JB (2016) An aqueous symmetric sodium-ion battery with NASICON-structured $Na_3MnTi(PO_4)_3$. Angew Chem Int Ed 55:12768–12772
19. Dong J, Zhang G, Wang X, Zhang S, Deng C (2017) Cross-linked $Na_2VTi(PO_4)_3$@C hierarchical nanofibers as high-performance bifunctional electrodes for symmetric aqueous rechargeable sodium batteries. J Mater Chem A 5:18725
20. Zhang F, Li W, Xiang X, Sun M (2017) Nanocrystal-assembled porous $Na_3MgTi(PO_4)_3$ aggregates as highly stable anode for aqueous sodium-ion batteries. Chem Eur J 23:12944–12948
21. Zheng W, Lei P, Luo D, Huang Y, Tian G, Xiang X (2020) Understanding the effect of structural compositions on electrochemical properties of titanium-based polyanionic compounds for superior sodium storage. Solid State Ionics 345:115194
22. Hu P, Wang X, Ma J, Zhang Z, He J, Wang X, Shi S, Cui G, Chen L (2016) $NaV_3(PO_4)_3$/C nanocomposite as novel anode material for Na-ion batteries with high stability. Nano Energy 26:382–391
23. Wang D, Bie X, Fu Q, Dixon D, Bramnik N, Hu YS et al (2017) Sodium vanadium titanium phosphate electrode for symmetric sodium-ion batteries with high power and long lifespan. Nat Commun 8:15888
24. Chen S, Wu C, Shen L, Zhu C, Yu Y (2017) Challenges and perspectives for NASICON-type electrode materials for advanced sodium-ion batteries. Adv Mater 29:1700431
25. Li H, Chen X, Jin T, Bao W, Zhang Z, Jiao L (2019) Robust graphene layer modified $Na_2MnP_2O_7$ as a durable high-rate and high energy cathode for Na-ion batteries. Energy Storage Mater 16:383–390
26. Li H, Jin T, Chen X, Lai Y, Jiao L (2018) Rational architecture design enables superior Na storage in greener NASICON-$Na_4MnV(PO_4)_3$ cathode. Adv Energy Mater 8:1801418
27. Saravanan K, Mason CW, Rudola A, Wong KH, Balaya P (2013) The first report on excellent cycling stability and superior rate capability of $Na_3V_2(PO_4)_3$ for sodium ion batteries. Adv Energy Mater 3:444–450
28. Zhou W, Xue L, Lü X, Gao H, John B (2016) Goodenough. $Na_xMV(PO_4)_3$ (M=Mn, Fe, Ni), structure and properties for sodium extraction. Nano Lett 16:7836–7841
29. Guo JZ, Wang PF, Wu XL, Zhang XH, Yan Q, Chen H et al (2017) High-energy/power and low-temperature cathode for sodium-ion batteries: in situ XRD study and superior full-cell performance. Adv Mater 29:1701968
30. Gao H, Li Y, Park K, Goodenough JB (2016) Sodium extraction from NASICON-structured $Na_3MnTi(PO_4)_3$ through Mn(III)/Mn(II) and Mn(IV)/Mn(III) redox couples. Chem Mater 28:6553–6559
31. Zhu T, Hu P, Wang X, Liu Z, Luo W, Owusu KA, Cao W, Shi C, Li J, Zhou L, Mai L (2019) Realizing three-electron redox reactions in NASICOM-structured $Na_3MnTi(PO_4)_3$ for sodium-ion batteries. Adv Energy Mater 9:1803436
32. Kumar PR, Jung YH, Lim CH, Kim DK (2015) $Na_3V_2O_{2x}(PO4)_2F_{3-2x}$: a stable and high-voltage cathode material for aqueous sodium-ion batteries with high energy density. J Mater Chem A 3:6271–6275
33. Shen W, Li H, Guo Z, Wang C, Li Z, Xu Q, Liu H, Wang Y, Xia Y (2016) Double nano-carbon synergistically modified $Na_3V_2(PO_4)_3$: an advanced cathode for high-rate and long-life sodium-ion batteries. ACS Appl Mater Interfaces 8:15341–15351
34. Liu S, Wang L, Liu J, Zhou M, Nian Q, Feng Y et al (2019) $Na_3V_2(PO_4)_2F_3$–SWCNT: a high voltage cathode for non-aqueous and aqueous sodium-ion batteries. J Mater Chem A 7:248–256
35. Zhang W, Zhang Z, Li H, Wang D, Wang T, Sun X, Zheng J, Lai Y (2019) Engineering 3D well-interconnected $Na_4MnV(PO_4)_3$ facilitates ultrafast and ultrastable sodium storage. ACS Appl Mater Interfaces 11:35746–35754
36. Sun C, Rajasekhara S, Dong Y, Goodenough JB (2011) Hydrothermal synthesis and electrochemical properties of $Li_3V_2(PO_4)(3)$/C-based composites for lithium-ion batteries. ACS Appl Mater Interfaces 3:3772–3776
37. Chao D, Lai CH, Liang P, Wei Q, Wang YS (2018) Sodium vanadium fluorophosphates (NVOPF) array cathode designed for high-rate full sodium ion storage device. Adv Energy Mater 8: 1800058
38. Zhao Y, Wang LP, Sougrati MT, Feng Z, Leconte Y, Fisher A, Srinivasan M, Xu Z (2017) A review on design strategies for carbon cased metal oxides and sulfides nanocomposites for high performance Li and Na ion battery anodes. Adv Energy Mater 7:1601424